JACS
JOURNAL OF THE AMERICAN CHEMICAL SOCIETY

Article

pubs.acs.org/JACS

Hot Electrons Generated from Doped Quantum Dots via Upconversion of Excitons to Hot Charge Carriers for Enhanced Photocatalysis

Yitong Dong,[†] Julius Choi,[§] Hae-Kwon Jeong,[§] and Dong Hee Son*,[†]

[†]Department of Chemistry, Texas A&M University, College Station, Texas 77843, United States

[§]Artie McFerrin Department of Chemical Engineering, Texas A&M University, College Station, Texas 77843, United States

Supporting Information

ABSTRACT: We show that hot electrons exhibiting the enhanced photocatalytic activity in H_2 production reaction can be efficiently generated in Mn-doped quantum dots via the "upconversion" of the energy of two excitons into the hot charge carriers. The sequential two-photon-induced process with the long-lived Mn excited state serving as the intermediate state is considered as the pathway generating hot electrons. H_2 production rate from doped quantum dots is significantly higher than that from undoped quantum dots and also exhibited the quadratic increase with the light intensity, demonstrating the effectiveness of the hot electrons produced in doped quantum dots in photocatalytic reaction. Due to the very long lifetime of Mn excited state (~6 ms) in the doped quantum dots, the sequential two-photon excitation requires relatively low excitation rates readily achievable with a moderately concentrated solar radiation, demonstrating their potential as an efficient source of hot electrons operating at low excitation intensities.

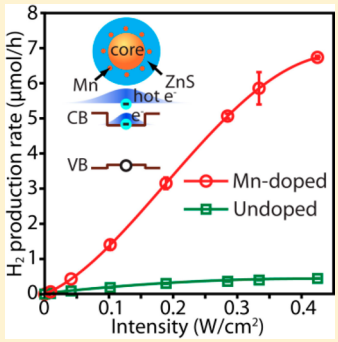

INTRODUCTION

Hot electrons in nanocrystals of semiconductors, metals, and their heterostructures received much attention due to their enhanced capability to undergo the interfacial charge transfer and induce the energetically expensive chemical reactions.[1−8] The excess energy of hot electrons lowers the energy barrier for the electron transfer facilitating the separation of charge carriers at the interface and interfacial electron transfer often faster than the relaxation of the electrons.[4,5,9] In simple semiconductor quantum dots, hot electrons can be produced via the excitation with the photons having higher energy than the bandgap. However, production of hot electrons with large excess energy using higher-energy photons is less desirable in the applications especially when using solar radiation as the light source, since it has a limited spectral coverage in the ultraviolet region. For this reason, much effort has been made to produce and utilize hot electrons efficiently without using high-energy photons. One strategy is using heterostructures with an appropriate combination of the conduction band offset and bandgap, where the electrons created in one side of the heterostructure by the bandgap excitation can be injected to the other side with excess kinetic energy.[5,10] Another strategy producing hot electrons is based on plasmon of the metal nanocrystals, where the nonradiative decay of plasmon can produce hot electrons above the Fermi level.[11−18] These hot electrons were utilized in various applications such as photocatalytic water splitting,[19−26] dissociation of H_2 molecules,[7,8] and photovoltaic devices.[11,13,16,27−30]

In this study, we showed that hot electrons can be generated in Mn-doped quantum dots via efficient "upconversion" of the energy of two excitons into a hot charge carriers with excess energy stored in the electron, showing the enhanced photocatalytic activity in H_2 production reaction. Such upconversion can be possible due to the very long lifetime (τ_{Mn} ~ 6 ms) of the Mn excited state sensitized via rapid exciton−Mn energy transfer, which can serve as a long-lived intermediate state for the sequential two-step process leading to the generation of hot electrons. The photophysical pathways in Mn-doped quantum dots that can potentially produce hot electrons have been recently proposed by us[31] and Gamelin's group,[32] both involving the Mn excited state as the intermediate state for the sequential two-step photoexcitation process. The proposed two-step process producing hot electrons is reminiscent of the photon upconversion in lanthanide-doped upconversion nanoparticles.[33,34] However, unlike in photon upconversion producing higher-energy photons, the energy of the absorbed photons in Mn-doped quantum dots is converted to hot charge carriers, whose excess energy can be utilized for a variety of chemical reactions as recently demonstrated with the plasmon-induced hot electrons.[17−24] Here we analyzed the photocatalytic H_2 production rates vs excitation intensity for both doped and undoped quantum dots to gain an insight into the mechanisms of the hot electron generation. H_2 production rate from doped quantum dots was not only higher than that from undoped quantum dots but also increased quadratically to the excitation intensity, in contrast to the linear increase for undoped quantum dots. These observations indicate that hot

Received: February 24, 2015
Published: April 10, 2015

DOI: 10.1021/jacs.5b02026
J. Am. Chem. Soc. 2015, 137, 5549−5554

electrons produced in doped quantum dots can be effectively harvested to enhance the photocatalytic reaction.

Another interesting aspect of Mn-doped quantum dots as a new source of hot electrons is the long lifetime of the intermediate state (τ_{Mn} = 10^{-3}–10^{-2} s). In principle, only a few hundred excitations per second in each particle are required to induce the sequential two-step process generating hot electrons. Such excitation rate can be achieved with the irradiance of moderately concentrated solar radiation in common colloidal quantum dots with the absorption cross section (σ) of >10^{-15} cm^2 in visible spectral range. In fact, Mn-doped quantum dots exhibited enhanced photocatalytic activity resulting from hot electrons under the excitation intensities comparable to several times the solar radiation. This demonstrates the doped quantum dots' potential as an efficient source of the hot electrons harvesting the solar radiation, when combined with other strategies to increase the excitation rate, such as the plasmon-enhancement of the excitation rate.

EXPERIMENTAL SECTION

Material Synthesis and Characterization. Undoped and Mn-doped CdSSe/ZnS core/shell quantum dots sharing the same host structures were synthesized following the well-established procedures published elsewhere.[35,36] CdSSe core was synthesized by injecting a 1-octadecene (ODE) solution of sulfur–selenium mixture (S:Se = 10:1, 2 mL) to the mixture of cadmium oxide (0.126 g), oleic acid (OA, 2.02 g), and ODE (12.0 mL) heated at 270 °C under nitrogen atmosphere. After 4 min of growth at 250 °C, the reaction was quenched to obtain the desired particle size (3.5 nm in diameter) and bandgap (500 nm for the band edge exciton absorption). The purified core was used for the subsequent synthesis of the core/shell quantum dots. For the synthesis of Mn-doped and undoped CdSSe/ZnS core/shell quantum dots, a well-established SILAR (successive ionic layer adsorption and reaction) method was used to coat ZnS shell as described in detail in our earlier work.[37] Briefly, an ODE solution of sulfur and ODE solution of zinc stearate were used as the precursor of sulfur and zinc, which were coated alternately on the surface of the core nanocrystals. The average thickness of the ZnS shell is 2.3 nm. In the case of Mn-doped CdSSe/ZnS quantum dots, Mn ions were introduced after coating two layers of the ZnS shell. Oleylamine (OAm) solution of manganese acetate was used as the precursor of Mn ion. After the incorporation of Mn ions, additional ZnS layers were coated after removing all the excess unreacted Mn ions to complete the coating of ZnS shell to the final thickness of 2.3 nm.

The resulting undoped and doped quantum dots further went through the exchange of the surface ligand to 3-mercaptopropionic acid (MPA) to make them water-soluble for photocatalytic H_2 production in water. This was achieved by mixing the quantum dot solution dispersed in chloroform with aqueous solution of MPA at pH > 8 and stirring overnight. TEM images of the final purified CdSSe core, undoped CdSSe/ZnS, and Mn-doped CdSSe/ZnS quantum dots are shown in Figure 1a–c. Elemental analysis employing ICP-MS was performed to determine the absorption cross section of each quantum dot sample shown in Figure 1d and the doping concentration (8 Mn ions/particle) in conjunction with the size information obtained from the TEM images. The detailed procedures are described in Supporting Information. The absorption spectra of the quantum dot solutions were obtained using a fiberoptic-coupled CCD spectrometer (USB4000, Ocean Optics). The lifetime of the Mn exited state, serving as the intermediate state in the upconversion process, was measured using a pulsed N_2 laser (NL100 SRS, 337 nm, 3.5 ns pulse width) as the excitation source and a PMT (R928, Hamamatsu) as the detector after selecting 610 ± 5 nm portion of the spectrum with a bandpass filter. (Figure S2 in Supporting Information)

Photocatalytic H_2 Production Rate Measurement. The photocatalytic H_2 production was performed in a Pyrex reactor enclosed by a Pyrex water jacket to keep the temperature of the sample

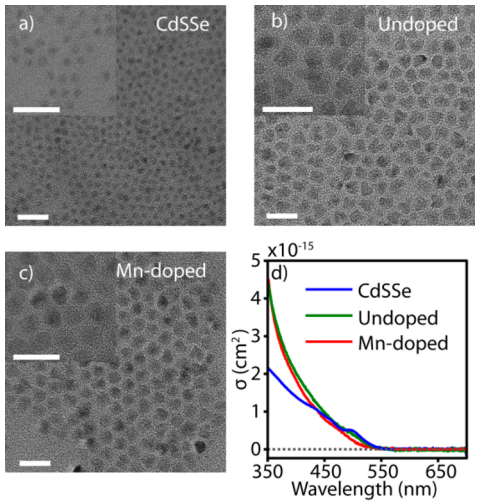

Figure 1. (a–c) TEM image of CdSSe core (a), undoped CdSSe/ZnS core/shell (b), and Mn-doped CdSSe/ZnS core/shell quantum dot (c). Scale bars are 20 nm. (d) Comparison of the absorption cross sections (σ) of the quantum dots.

solution constant at 10 °C. The details of the construction are in Supporting Information. The reactor contained 60 mL of the aqueous solution of the quantum dots and 0.05 M Na_2SO_3/0.05 M Na_2S added as the sacrificial hole scavenger. The pH of the solution was kept at 12. A 300 W xenon lamp (PerkinElmer PE300BF), providing light in the spectral range of 375–730 nm, was used as the excitation source. Before the reaction, the solution in the reactor was purged with Ar gas for 30 min to remove the oxygen. The intensity of the Xe light source at the sample reactor was controlled by varying the distance between the light source with a finite beam divergence and the reactor using the translation stage for the accurate and reproducible control of the light intensity. Pyroelectric power meter (Ophir, Nova) was used to measure the spatial distribution of the light intensity at the reactor location. From the measured total light intensity (W/cm^2) and the relative spectral irradiance measured with a spectrally calibrated spectrometer, photon irradiance (no. of photons/s·cm^2·nm) required for calculating the excitation rate was obtained as described in detail in Supporting Information. The amount of H_2 gas produced from the reaction was quantified by using gas chromatography (Agilent 3000A microGC, Molecular sieve 5A, TCD detector, Ar carrier gas). The concentration of the H_2 gas was measured at five different times during the reaction, and the linear slope was taken as the H_2 production rate. The measurements were repeated multiple times using the fresh quantum dot samples from the same batch to obtain the statistical error bar.

RESULTS AND DISCUSSION

Figure 2a shows the optical absorption spectra of undoped and Mn-doped CdSSe/ZnS core/shell quantum dots used to investigate the hot electron generation in doped quantum dots from the comparison of the H_2 production rate vs excitation intensity. Since both doped and undoped quantum dots share the same host structure and the dopant has little absorption, their absorption spectra are very similar. Core/shell structure of the host serves two purposes in this study. First, CdSSe with the lower band gap is the superior light absorber, while ZnS provides the more favorable local environment that can maximize the Mn excited state lifetime. By using the core/shell structure with dopant ions confined in the shell region, the structural variables influencing the absorption of exciton and excited state dynamics of Mn can be independently controlled. Second, the conduction band offset between the core and shell allows a facile distinction between hot electrons and the lower-

DOI: 10.1021/jacs.5b02026
J. Am. Chem. Soc. 2015, 137, 5549–5554

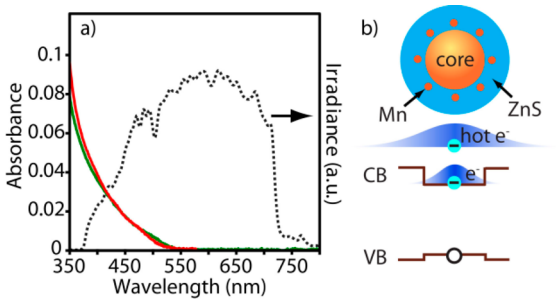

Figure 2. (a) Absorption spectra of undoped (green) and Mn-doped (red) CdSSe/ZnS quantum dot sample solutions used for H_2 production in a 1 cm-thick cuvette. The broken line is the irradiance of the Xe light source. (b) (top) Schematic representation of the doped quantum dot structure, and (bottom) comparison of the spatial extent of hot electron and band edge electron in conduction band.

energy electrons from one-photon-excited exciton. The conduction band offset at the core/shell interface (~0.5 eV) creates an energy barrier for the electrons from the exciton, while hot electrons have sufficient excess energy to overcome the barrier as illustrated in Figure 2b. Therefore, hot electrons are preferentially represented in the photocatalytic reaction products, i.e., H_2 produced from the reduction of proton,[38,39] detected from doped quantum dots.

Superimposed on the absorption spectra in Figure 2a is the spectral irradiance of the Xe light source used for the photoexcitation, which covers the spectral range of 375−730 nm mimicking the UV−visible component of the solar radiation. The solutions of both quantum dot samples were prepared such that they have the same total photon absorption rate (R_{ph}) determined by the absorbance, $A(\lambda)$, of the sample and the spectral photon irradiance, $I_{ph}(\lambda)$, of the light source by evaluating $R_{ph} \propto \int (1-10^{-A(\lambda)}) I_{ph}(\lambda)\, d\lambda$. Since both doped and undoped quantum dots were synthesized using the same CdSSe core, their absorption cross sections are very close in the spectral region that absorbs the photons from the Xe light source. This ensures that the ratio of the experimentally measured H_2 production rates from the two quantum dot samples directly reflects the ratio of the efficiency of the photocatalytic reaction.

Figure 3a compares the H_2 production rates from the aqueous solutions of doped ($R_{H2,d}$) and undoped ($R_{H2,ud}$) CdSSe/ZnS quantum dots in the presence of sacrificial hole

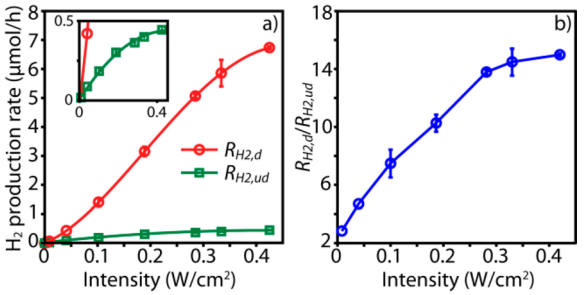

Figure 3. (a) H_2 production rate for doped ($R_{H2,d}$, red) and undoped ($R_{H2,ud}$, green) CdSSe/ZnS quantum dots vs excitation light intensity. Inset shows the magnified view of $R_{H2,ud}$. The error bar is smaller than the size of the marker if not indicated. (b) The ratio of two H_2 evolution rates ($R_{H2,d}/R_{H2,ud}$) vs excitation light intensity. Solid curves are guides to eyes.

scavenger (0.05 M Na_2S and 0.05 M Na_2SO_3) at pH of 12 as a function of the average excitation intensity at the sample. The ratio of the two H_2 production rates from doped and undoped quantum dots ($R_{H2,d}/R_{H2,ud}$) is shown in Figure 3b. A clearly visible trend is that $R_{H2,d}$ of doped quantum dots is significantly larger than $R_{H2,ud}$ of undoped quantum dots. In undoped quantum dots, the electrons from excitons are responsible for the production of H_2. In doped quantum dots, the population of exciton is diminished due to the energy transfer to Mn, contributing less to the production of H_2 than in undoped quantum dots. Therefore, the majority of H_2 produced by doped quantum dots should be accounted for by more reactive species than the electrons from exciton, i.e., hot electrons, as will be discussed further below.

A more interesting difference between $R_{H2,d}$ and $R_{H2,ud}$ is their dependence on the light intensity. $R_{H2,ud}$ exhibits initially a linear increase at the intensities below 0.2 W/cm^2 and a sublinear increase at the higher intensities as shown in the inset of Figure 3a. On the other hand, $R_{H2,d}$ exhibits a superlinear increase initially, while the slope becomes less steep at the higher intensities. The different intensity dependence of $R_{H2,d}$ and $R_{H2,ud}$ is more distinct in their ratio shown in Figure 3b. The values of $R_{H2,d}/R_{H2,ud}$ increases linearly from 3 to 14 in the intensity range of 0.01−0.33 W/cm^2. Since the production of H_2 by undoped quantum dots results from the one-photon-excited exciton, the linear increase of $R_{H2,d}/R_{H2,ud}$ with light intensity indicates the $R_{H2,d}$ increases quadratically to the light intensity via two-photon process in doped quantum dots. At these excitation intensities, creating hot electrons via direct two-photon excitation of hot exciton is highly unlikely. Therefore, the signature of the two-photon process observed here can be explained only by the proposed sequential two-photon process involving Mn excited state as the long-lived intermediate state. Furthermore, the values of $R_{H2,d}/R_{H2,ud}$ significantly larger than 1 indicates that hot electrons exhibiting much stronger reactivity than the electrons from exciton can be efficiently harvested competing with the relaxation of hot electrons to the band edge.

To confirm the feasibility of producing hot electrons via the sequential two-photon absorption through the excited Mn state as the intermediate state under our excitation condition, the rate of excitation was estimated within the excitation intensity range of this study. Based on the experimentally measured absorption cross section of Mn-doped quantum dots, the average rate of excitation in each doped quantum dot was determined to be 6−262/s in the excitation intensity range of this study (0.01−0.425 W/cm^2). See Supporting Information for details of calculation. This corresponds to the average excitation rate of $0.03-1.52/\tau_{Mn}$ in each quantum dot for the Mn excited state lifetime of τ_{Mn} = 5.8 ms. The Poisson probabilities ($P_n \geq 2$) of two or more excitations during τ_{Mn}, required to produce hot electrons, are shown in Figure 4. It is noteworthy that P_2 and P_3 carrying the appreciable probabilities exhibit a superlinear increase at the lower light intensities while it becomes more linear at the higher intensities similarly to $R_{H2,d}$ shown in Figure 3a. This observation strongly supports that the quadratic increase of $R_{H2,d}$ with the light intensity results from the process involving the sequential two-photon absorption during the lifetime of the intermediate state. It is also worth to mention that the intensity of light used to produce hot electrons in doped quantum dots in this study is comparable to the moderately concentrated solar radiation and significantly lower than those used in several recent studies of

DOI: 10.1021/jacs.5b02026
J. Am. Chem. Soc. 2015, 137, 5549−5554

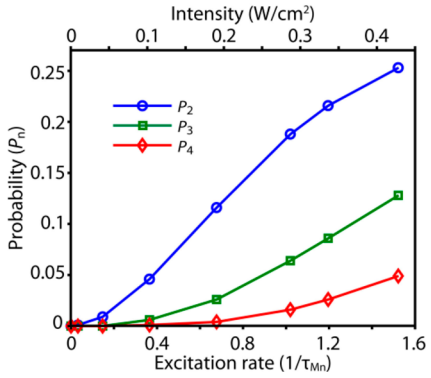

Figure 4. Poisson probability of two to four excitations during τ_{Mn} in doped quantum dots as a function of the average excitations rate and light intensity.

plasmon-induced hot electron generation.[21,34,40] The Xe light source used in this study delivers approximately twice the irradiance of AM1.5 in the same spectral range at the intensity of 0.1 W/cm^2. This suggests the possibility of generating hot electrons from natural solar radiation with an additional improvement of the excitation rate via, for example, plasmon-enhanced excitation. The quantum yield of H_2 production is ~0.3% and ~0.03% for doped and undoped quantum dots, respectively, at 0.2 W/cm^2, whose relatively low absolute values are due to the high pH of the solution used in this study.

We also compared the H_2 production rates from doped CdSSe/ZnS quantum dots ($R_{H2,d}$) and undoped CdSSe core quantum dots ($R_{H2,core}$) without the ZnS shell as shown in Figure 5a. The concentrations of the quantum dot solutions

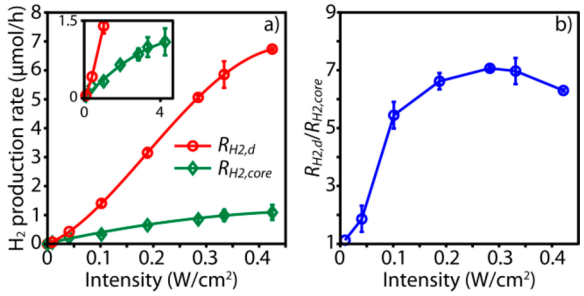

Figure 5. (a) H_2 production rate for doped CdSSe/ZnS quantum dots ($R_{H2,d}$, red) and undoped CdSSe core quantum dots ($R_{H2,core}$, green) vs excitation intensity. Inset shows the magnified view of $R_{H2,core}$. The error bar is smaller than the size of the marker if not indicated. (b) The ratio of H_2 evolution rates ($R_{H2,d}/R_{H2,core}$) vs excitation intensity. Solid curves are guides to eyes.

were adjusted such that both absorb the same amount of photons. Undoped core quantum dots exhibit a H_2 production rate higher than that of undoped core/shell quantum dots due to the absence of the shell that functions as the energy barrier for the electrons. However, doped quantum dots are still superior in photocatalytic activity compared with undoped core quantum dots. The ratio of the two H_2 production rates ($R_{H2,d}/R_{H2,core}$) exhibits an increase with the light intensity at lower intensity ranges similarly to Figure 3b. These results strongly indicate that hot electrons exhibiting the enhanced reducing capability are produced in doped quantum dots via the process involving consecutive two-photon absorption as previously proposed.

To gain a further mechanistic insight into the hot electron generation, we consider a simple model describing the major kinetic pathways in photoexcited Mn-doped quantum dots shown in Figure 6. We will also examine the structural

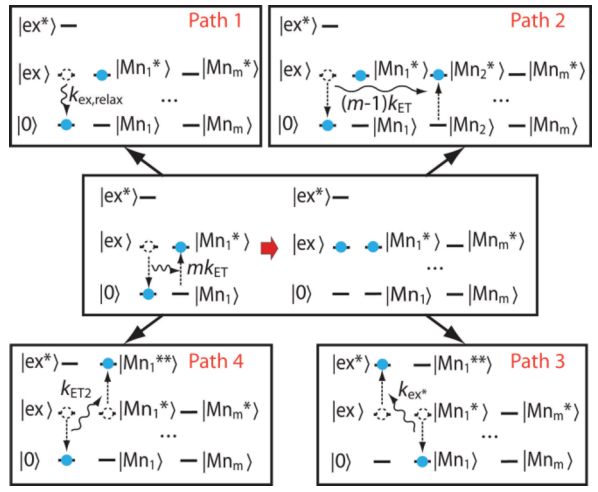

Figure 6. Kinetic scheme showing four major pathways in Mn-doped quantum dots after the sequential excitation of two excitons. Doping concentration is m dopant ions/particle. |0⟩, |ex⟩, and |ex*⟩ represent the ground, exciton, and hot electron state of the host quantum dot, respectively. |Mn⟩, |Mn*⟩, and |Mn**⟩ represent the ground, excited, and the higher excited state of doped Mn ions, respectively.

correlation of the relative efficiency of the paths leading to the generation of hot electrons based on this model, which bears a practical important in future studies utilizing doped quantum dots as an efficient source of hot electrons. Figure 6 shows four competing kinetic paths in Mn-doped quantum dots when the second photon excites an exciton in the presence of one Mn excited state created by the first photon via exciton-Mn energy transfer. |0⟩, |ex⟩, and |ex*⟩ represent the ground state, exciton, and hot exciton carrying the excess energy in electron, respectively. |Mn⟩, |Mn*⟩, and |Mn**⟩ represent the ground, excited, and higher excited state of Mn, respectively. In this scheme, the relaxation of |ex*⟩ and |M**⟩ and the transfer of hot electron to the electron acceptors are not included, since we focus on examining the branching ratio of the paths leading to the generation of hot electrons competing with other processes, rather than performing a full quantitative kinetic modeling.

Path 1 represents the relaxation of exciton including the trapping of exciton, leaving one |Mn*⟩. Path 2 represents the energy transfer from exciton to Mn that results in two |Mn*⟩. Both of these two paths do not create hot electrons. On the other hand, paths 3 and 4 were previously proposed to be responsible for the generation of hot electrons.[31,32] In path 3, hot electrons are produced by the Auger type cross relaxation, where ~2 eV of energy from |Mn*⟩ is transferred to the electron in the conduction band. The net result of path 3 is converting two excitons into one hot exciton with the electron carrying ~2 eV of excess energy in the conduction band. In path 4, on the other hand, the energy of exciton is transferred to the existing |Mn*⟩ creating |M**⟩. Our earlier study proposed that creating |M**⟩ is equivalent to producing a hot electron in the conduction band of the host and a localized hole at the Mn site.[31] This possibility was questioned in ref 32 based on the earlier photoelectron spectroscopy data suggesting that

DOI: 10.1021/jacs.5b02026
J. Am. Chem. Soc. 2015, 137, 5549−5554

the excited d electron in |M**⟩ may lie below the valence band edge, while there still remains some uncertainty in the energetic location of the excited d electrons in |M**⟩. However, path 4 may still generate hot electrons via the energy transfer from |M**⟩ to create |ex*⟩ regardless of the energetic location of the excited electron in |M**⟩. Such a process is plausible since the time for relaxation from |M**⟩ to |Mn*⟩ is considered to be generally slow due to the very weak optical transition dipole between Mn ligand field states, possibly orders of magnitude slower than the time scale of the exciton−Mn energy transfer. In Mn-doped CdS/ZnS quantum dots having the similar size and structure as Mn-doped CdSSe/ZnS quantum dots used in this study, the energy transfer between exciton and one Mn ion was measured to be ∼200 ps,[37] whereas the time scale of several hundred microseconds was reported for the relaxation between the low-lying excited states of Mn ions doped in ZnS.[41] Assuming that the dynamics of the energy transfer involving |M**⟩ and |ex*⟩ are similar to their lower-energy counterparts, path 4 can also generate hot electrons.

The branching ratio of each path in Figure 6 can be expressed as follows. While some rate constants are only approximate, we evaluated the branching ratio of each path for the case of $m = 8$, the average doping concentration of the doped quantum dots used in this study.

$$\text{path 1: } k_{ex,relax}/[k_{ex,relax} + (m-1)k_{ET} + k_{ex^*} + k_{ET2}] = 18.2\%$$

$$\text{path 2: } (m-1)k_{ET}/[k_{ex,relax} + (m-1)k_{ET} + k_{ex^*} + k_{ET2}] = 63.6\%$$

$$\text{path 3: } k_{ex^*}/[k_{ex,relax} + (m-1)k_{ET} + k_{ex^*} + k_{ET2}] = 9.1\%$$

$$\text{path 4: } k_{ET2}/[k_{ex,relax} + (m-1)k_{ET} + k_{ex^*} + k_{ET2}] = 9.1\%$$

The relaxation rate of exciton ($k_{ex,relax} = 10^{10}$ s^{-1}) reflecting both the radiative and nonradiative decay and the energy transfer rate ($k_{ET} = 5 \times 10^9$ s^{-1}) between a single pair of exciton and Mn ion were taken from our recent pump−probe study on Mn-doped CdS/ZnS quantum dots having a structure similar to the doped quantum dots used in this study. Since the overall rate of the exciton-Mn energy transfer is proportional to the number of Mn ions in its ground state, preparation of |Mn*⟩ from the first photon absorption can be very efficient for the doped quantum dots with a multiple number of dopant ions. The Auger cross relaxation rate (k_{ex^*}) is uncertain, while it is expected to be of similar order of magnitude to k_{ET} or larger.[30] k_{ET2}, the rate of energy transfer from |ex⟩ to |Mn*⟩, is assumed to be similar to k_{ET}, although it can also be larger than k_{ET} due to the stronger transition dipole for the excited state absorption than the ground state absorption of the doped Mn ions. Under the assumption that $k_{ex^*} = k_{ET} = k_{ET2}$, the combined branching ratio of paths 3 and 4 that can generate hot electrons is ∼20%. While this calculation is only approximate, it demonstrates that the probability of generating hot electrons via two sequential excitations is significant. In the case of three or more excitations during τ_{Mn}, a more complex kinetic scheme should be considered. However, the net effect is creating more |Mn*⟩, which will increase the probability of creating hot electrons even more.

Since the rates of various dynamic processes that determine the efficiency of hot electron generation can be tuned by varying the structure of the doped quantum dots, we will briefly discuss the expected effect of several structural variations. This will be important for future efforts to optimize the structure of the doped quantum dots to maximize the hot electron generation efficiency. On the basis of the above kinetic model, the branching ratios of paths 3 and 4 become larger with smaller m, i.e., lower doping concentration. This suggests that if the energy transfer from the first photon absorption creating |Mn*⟩ is sufficiently fast compared to $k_{ex,relax}$, hot electron generation will be more efficient at lower doping concentrations. In reality, because the doping concentration affects the dynamics of both the first and second steps of the two-step process shown in Figure 6, in the opposite directions for paths 3 and 4, there should be an optimum doping concentration that maximizes the probability of hot electron generation. Another important parameter is the excitation rate per particle at a given excitation light intensity. A straightforward way to increase the excitation rate is increasing the absorption cross section by increasing the volume of the quantum dot or adding other sensitizers. Plasmon-enhancement of the excitation rate will also be useful, since the generation of hot electron can be achieved with a weaker light source, analogous to the plasmon-enhanced luminescence demonstrated in various molecular luminophores and quantum dots. Furthermore, the recently observed resistance of |Mn*⟩ to nonradiative quenching by the plasmonic metal nanocrystals will be particularly advantageous when utilizing plasmon to enhance the hot electron generation capability of doped quantum dots.[42]

CONCLUSION

We showed that hot electrons exhibiting enhanced photocatalytic activity are produced in Mn-doped quantum dots via the efficient upconversion of the energy of two excitons into hot charge carriers, taking advantage of the very long lifetime of the Mn excited state. The rate of H_2 production by Mn-doped quantum dots exhibited a quadratic increase with excitation light intensity, whereas a linear increase was observed in undoped quantum dots, indicating the involvement of a two-photon-induced process. The analysis of the excitation rate vs light intensity supports the sequential two-step mechanism leading to the generation of hot electrons via a very long-lived Mn excited state as the intermediate state. Two different pathways, both sharing the same Mn intermediate state, have been considered responsible for generating hot electrons in Mn-doped quantum dots. This study also indicates that Mn-doped quantum dots can potentially be a highly efficient source of hot electrons operating at very low excitation intensities, when the longevity of the Mn excited state is combined with the other strategies, such as plasmon enhancement of the excitation rate. Furthermore, the upconversion of excitons producing hot electrons observed in this study suggests a possible production of hot holes in the structures with efficient coupling between hole and Mn, which may further expand the utility of the hot charge carriers.

ASSOCIATED CONTENT

Supporting Information

Determination of absorption cross section and doping concentration, calculation of photon irradiance and average rate of excitation in each quantum dot, experimental setup for

DOI: 10.1021/jacs.5b02026
J. Am. Chem. Soc. 2015, 137, 5549−5554

the measurement of the H_2 production rate, luminescence spectra of Mn-doped quantum dots, and photoluminescence lifetime measurement of Mn excited state. This material is available free of charge via the Internet at http://pubs.acs.org.

AUTHOR INFORMATION

Corresponding Author

*dhson@chem.tamu.edu.

Notes

The authors declare no competing financial interest.

ACKNOWLEDGMENTS

This work was supported by NSF (CBET-1264840).

REFERENCES

(1) Furube, A.; Du, L.; Hara, K.; Katoh, R.; Tachiya, M. *J. Am. Chem. Soc.* **2007**, *129*, 14852.
(2) Wu, K.; Rodriguez-Cordoba, W. E.; Yang, Y.; Lian, T. *Nano Lett.* **2013**, *13*, 5255.
(3) Pandey, A.; Guyot-Sionnest, P. *J. Phys. Chem. Lett.* **2010**, *1*, 45.
(4) Tisdale, W. A.; Williams, K. J.; Timp, B. A.; Norris, D. J.; Aydil, E. S.; Zhu, X. Y. *Science* **2010**, *328*, 1543.
(5) Williams, K. J.; Nelson, C. A.; Yan, X.; Li, L. S.; Zhu, X. Y. *ACS Nano* **2013**, *7*, 1388.
(6) Sippel, P.; Albrecht, W.; Mitoraj, D.; Eichberger, R.; Hannappel, T.; Vanmaekelbergh, D. *Nano Lett.* **2013**, *13*, 1655.
(7) Mukherjee, S.; Zhou, L. A.; Goodman, A. M.; Large, N.; Ayala-Orozco, C.; Zhang, Y.; Nordlander, P.; Halas, N. J. *J. Am. Chem. Soc.* **2014**, *136*, 64.
(8) Mukherjee, S.; Libisch, F.; Large, N.; Neumann, O.; Brown, L. V.; Cheng, J.; Lassiter, J. B.; Carter, E. A.; Nordlander, P.; Halas, N. J. *Nano Lett.* **2013**, *13*, 240.
(9) Son, D. H.; Wittenberg, J. S.; Alivisatos, A. P. *Phys. Rev. Lett.* **2004**, *92*, 127406.
(10) Yang, Y.; Lian, T. *Coord. Chem. Rev.* **2014**, *263*, 229.
(11) Manjavacas, A.; Liu, J. G.; Kulkarni, V.; Nordlander, P. *ACS Nano* **2014**, *8*, 7630.
(12) Baffou, G.; Quidant, R. *Chem. Soc. Rev.* **2014**, *43*, 3898.
(13) Brongersma, M. L.; Halas, N. J.; Nordlander, P. *Nat. Nanotechnol.* **2015**, *10*, 25.
(14) Clavero, C. *Nat. Photonics* **2014**, *8*, 95.
(15) Avanesian, T.; Christopher, P. *J. Phys. Chem. C* **2014**, *118*, 28017.
(16) Knight, M. W.; Sobhani, H.; Nordlander, P.; Halas, N. J. *Science* **2011**, *332*, 702.
(17) Marchuk, K.; Willets, K. A. *Chem. Phys.* **2014**, *445*, 95.
(18) Linic, S.; Christopher, P.; Xin, H. L.; Marimuthu, A. *Acc. Chem. Res.* **2013**, *46*, 1890.
(19) Yu, S.; Kim, Y. H.; Lee, S. Y.; Song, H. D.; Yi, J. *Angew. Chem., Int. Ed.* **2014**, *53*, 11203.
(20) Chen, H. M.; Chen, C. K.; Chen, C.-J.; Cheng, L.-C.; Wu, P. C.; Cheng, B. H.; Ho, Y. Z.; Tseng, M. L.; Hsu, Y.-Y.; Chan, T.-S.; Lee, J.-F.; Liu, R.-S.; Tsai, D. P. *ACS Nano* **2012**, *6*, 7362.
(21) DuChene, J. S.; Sweeny, B. C.; Johnston-Peck, A. C.; Su, D.; Stach, E. A.; Wei, W. D. *Angew. Chem., Int. Ed.* **2014**, *53*, 7887.
(22) Kang, Y.; Gong, Y.; Hu, Z.; Li, Z.; Qiu, Z.; Zhu, X.; Ajayan, P. M.; Fang, Z. *Nanoscale* **2015**, *7*, 4482.
(23) Ingram, D. B.; Linic, S. *J. Am. Chem. Soc.* **2011**, *133*, 5202.
(24) Murdoch, M.; Waterhouse, G. I. N.; Nadeem, M. A.; Metson, J. B.; Keane, M. A.; Howe, R. F.; Llorca, J.; Idriss, H. *Nat. Chem.* **2011**, *3*, 489.
(25) Warren, S. C.; Thimsen, E. *Energy Environ. Sci.* **2012**, *5*, 5133.
(26) Mubeen, S.; Lee, J.; Singh, N.; Kramer, S.; Stucky, G. D.; Moskovits, M. *Nat. Nanotechnol.* **2013**, *8*, 247.
(27) Sil, D.; Gilroy, K. D.; Niaux, A.; Boulesbaa, A.; Neretina, S.; Borguet, E. *ACS Nano* **2014**, *8*, 7755.
(28) Atar, F. B.; Battal, E.; Aygun, L. E.; Daglar, B.; Bayindir, M.; Okyay, A. K. *Opt. Express* **2013**, *21*, 7196.
(29) Mubeen, S.; Hernandez-Sosa, G.; Moses, D.; Lee, J.; Moskovits, M. *Nano Lett.* **2011**, *11*, 5548.
(30) Wang, F. M.; Melosh, N. A. *Nano Lett.* **2011**, *11*, 5426.
(31) Chen, H. Y.; Chen, T. Y.; Berdugo, E.; Park, Y.; Lovering, K.; Son, D. H. *J. Phys. Chem. C* **2011**, *115*, 11407.
(32) Bradshaw, L. R.; Hauser, A.; McLaurin, E. J.; Gamelin, D. R. *J. Phys. Chem. C* **2012**, *116*, 9300.
(33) Wang, F.; Liu, X. G. *Chem. Soc. Rev.* **2009**, *38*, 976.
(34) Gamelin, D. R.; Gudel, H. U. *Transition Metal and Rare Earth Compounds: Excited States, Transitions, Interactions II*; Springer: New York, 2001; Vol. *214*, p 1.
(35) Yang, Y. A.; Chen, O.; Angerhofer, A.; Cao, Y. C. *J. Am. Chem. Soc.* **2008**, *130*, 15649.
(36) Hsia, C. H.; Wuttig, A.; Yang, H. *ACS Nano* **2011**, *5*, 9511.
(37) Chen, H. Y.; Maiti, S.; Son, D. H. *ACS Nano* **2012**, *6*, 583.
(38) Chen, X. B.; Shen, S. H.; Guo, L. J.; Mao, S. S. *Chem. Rev.* **2010**, *110*, 6503.
(39) Osterloh, F. E. *Chem. Soc. Rev.* **2013**, *42*, 2294.
(40) Zhang, Z. L.; Sheng, S. X.; Zheng, H. R.; Xu, H. X.; Sun, M. T. *Nanoscale* **2014**, *6*, 4903.
(41) Kushida, T.; Tanaka, Y.; Oka, Y. *Solid State Commun.* **1974**, *14*, 617.
(42) Park, Y.; Pravitasari, A.; Raymond, J. E.; Batteas, J. D.; Son, D. H. *ACS Nano* **2013**, *7*, 10544.

DOI: 10.1021/jacs.5b02026
J. Am. Chem. Soc. 2015, 137, 5549−5554